SR investigation of magnetism and magnetoelectric coupling in Cu_2OSeO_3

Maisuradze, A ; Guguchia, Z ; Graneli, B ; Rønnow, H M ; Berger, H ; Keller, H

Abstract: A detailed zero- and transverse-field muon spin rotation investigation of magnetism and the magnetoelectric coupling in Cu2OSeO3 is reported. An internal magnetic field Bint(T=0)=85.37(25) mT was found, in agreement with a ferrimagnetic state below Tc=57.0(1) K. The temperature dependence of the magnetic order parameter is well described by the relation Bint=B(0)(1−(T/Tc)2)˜ with an effective exponent ˜ 0.39(1), which is close to the critical exponent 1/3 for a three-dimensional (3D) magnetic system. Just above Tc the muon relaxation rate follows the power law (T) (T/Tc−1)−˜ with ˜=1.06(9), which is characteristic for 3D ferromagnets. Measurements of Bint(T) with and without an applied electrostatic field E=1.66×105 V/m suggest a possible electric-field effect of magnitude ΔBV=BV(0 V)−BV(500 V)=−0.4(4) mT. ©2011 American Physical Society

DOI: https://doi.org/10.1103/PhysRevB.84.064433

μSR investigation of magnetism and magnetoelectric coupling in Cu_2OSeO_3

A. Maisuradze,[1,2,*] Z. Guguchia,[1] B. Graneli,[1,3] H. M. Rønnow,[4] H. Berger,[4] and H. Keller[1]

[1] *Physik-Institut der Universität Zürich, Winterthurerstrasse 190, CH-8057 Zürich, Switzerland*
[2] *Laboratory for Muon Spin Spectroscopy, Paul Scherrer Institut, CH-5232 Villigen PSI, Switzerland*
[3] *Institute of Theoretical Physics, ETH Hönggerberg, CH-8093 Zürich, Switzerland*
[4] *Institute of Condensed Matter Physics, École Polytechnique Fédérale de Lausanne (EPFL), CH-1015 Lausanne, Switzerland*

A detailed zero and transverse field (ZF&TF) muon spin rotation (μSR) investigation of magnetism and the magneto-electric coupling in Cu_2OSeO_3 is reported. An internal magnetic field $B_{\rm int}(T=0) = 85.37(25)$ mT was found, in agreement with a ferrimagnetic state below $T_{\rm c} = 57.0(1)$ K. The temperature dependence of the magnetic order parameter is well described by the relation $B_{\rm int} = B(0)(1-(T/T_{\rm c})^2)^{\tilde{\beta}}$ with an effective exponent $\tilde{\beta} \simeq 0.39(1)$ which is close to the critical exponent $\beta \simeq 1/3$ for a three dimensional (3D) magnetic system. Just above $T_{\rm c}$ the muon relaxation rate follows the power low $\lambda(T) \propto (T/T_{\rm c}-1)^{-\tilde{\omega}}$ with $\tilde{\omega} = 1.06(9)$, which is characteristic for 3D ferromagnets. Measurements of $B_{\rm int}(T)$ with and without an applied electrostatic field $E = 1.66\times10^5$ V/m suggest a possible electric field effect of magnitude $\Delta B_V = B_V(0\text{V}) - B_V(500\text{V}) = -0.4(4)$ mT.

PACS numbers:

I. INTRODUCTION

Much attention has been directed toward multiferroic and magnetoelectric materials in recent years.[1–4] The coupling between magnetic and electric parameters increases the degrees of freedom of the ordered ground state, making these materials good candidates for the study of new phenomena in highly correlated electronic systems. Strong magnetoelectric coupling is rather rare in the solid state, since usual microscopic mechanisms for magnetic and electric polarization are mutually exclusive. Magnetism requires strong exchange interactions related to a strong hybridization of the transition ion electrons leading to conductivity. Conductivity, on the other hand, is inconsistent with the presence of an electric polarization in a sample.[5] It is therefore of particular importance to unravel the mechanisms behind magnetoelectric coupling. A number of atomic mechanisms have been proposed in order to explain the magnetoelectric coupling.[1,6–8] Considering spatial and time inversion symmetry for the magnetic ($\mathbf{M}$) and the electric ($\mathbf{P}$) polarization, it was concluded that linear magnetoelectric coupling is only possible when both vectors vary in space and time.[4] On the other hand, the importance of frustration effects in magnetoelectrics for the static polarizations of $\mathbf{P}$ and $\mathbf{M}$ was stressed for nonlinear coupling mechanisms.[4] The presence of large magnetic and electric polarizations is an important condition for strong magnetoelectric coupling, making ferro- or ferrimagnetic materials favorable candidates.[1]

The ferrimagnetic magnetoelectric compound Cu_2OSeO_3 was recently discovered,[9,10] and single crystals were successfully grown soon after.[11] The compound is piezoelectric and undergoes a ferrimagnetic transition below 60 K, exhibiting magnetoelectric coupling as revealed by magneto-capacitance studies on a polycrystalline sample.[9] An abrupt change of the dielectric constant below the ferrimagnetic transition was later confirmed by infrared studies.[12,13] At present the nature of the magnetoelectric coupling is unknown, since the most common mechanisms, involving magnetostriction and piezoelectric effects via lattice distortions are excluded. Neither X-ray diffraction (XRD)[9] nor nuclear magnetic resonance (NMR)[11] studies revealed any lattice anomaly below the Néel temperature.

The positive muon is a very sensitive microscopic probe for studying magnetic properties in zero as well as in an applied electric field.[14] Following the pioneering works of Eschchenko *et al.*[15] and Lewtas *et al.*[16] we implemented a setup with alternating electric fields, and performed a muon spin rotation/relaxation (μSR) investigation of magnetism and magnetoelectric coupling in Cu_2OSeO_3. The temperature dependence of the internal magnetic field $B_{\rm int}$ was investigated below $T_{\rm c} = 57.0(1)$ K, and the relaxation rate was studied above $T_{\rm c}$. Zero field μSR measurements of the internal field distribution with and without an applied electric field $E = 1.66\times10^5$ V/m indicate a small electric field effect on the internal magnetic field: $\Delta B_V = B_V(0\text{V}) - B_V(500\text{V}) = -0.4(4)$ mT.

The paper is organized as follows: The sample preparation and the details of experimental setup are described in Sec. II. In Sec. III we describe the model used for the analysis of the μSR data and the relation of the measured μSR spectrum to the lattice and magnetic structure of the sample. In Sec. IV we present and discuss the obtained results. Conclusion is given in Sec. V.

II. EXPERIMENTAL DETAILS

A high quality single crystal of Cu_2OSeO_3 of approximate size $7\times8\times3$ mm^3 was prepared in a manner described elsewhere.[11] The zero field (ZF) and transverse field (TF) μSR experiments were performed at the πE3 beam line at the Paul Scherrer Institute (Villigen, Switzerland). The crystal structure is cubic with symmetry ($P2_13$).[9,10] The sample was aligned with its (100) direction parallel to the incident muon beam. The spin

vector of the muon was oriented approximately with an angle of 60 degrees with respect to the momentum vector. The asymmetry time spectra were monitored in the "Forward", "Backward", "Up", and "Down" (FBUD) positron detectors.[14] Typical statistics was 40 to 50×10^6 positron events in the FBUD detectors for a spectrum with a 5 μs time window. The switched electric field E was applied along the (100) direction of the 3 mm thick crystal. The crystal was mounted between two Cu electrodes: A thin (50μm) Cu metal foil was used as the positive electrode, and the negative electrode was soldered to the sample holder and electrically connected to ground. The applied voltage was switched at a rate of 100 Hz for two reasons: (i) to avoid accumulation of muon created charge in the vicinity of the sample-to-electrode contact surface, which might offset and even cancel the applied field E, and (ii) to provide a well-defined consecutive reference in order to reduce artefacts related to any slight variation in temperature or applied magnetic field with time. All the positron events registered by the FBUD detectors were stored alternatively in the first block of four histograms when the electric field was off, and the second block of four histograms when the electric field was on. Measurements were performed for two different electric fields: $E = 500/3$ V/mm and $E = 800/3$ V/mm (i.e. 500 or 800 V applied on 3 mm thick sample).

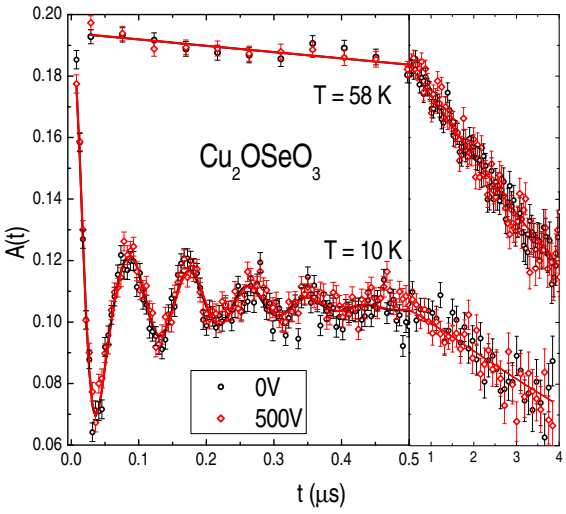

FIG. 1: (Color online) μSR time spectra of Cu_2OSeO_3 at 10 and 58 K in ZF with ($\diamond$) and without ($\circ$) applied electrical field $E = 500/3$ V/mm. Solid lines are fits to the data using Eqs. (2) and (3).

III. ANALYSIS AND MODELS

ZF μSR allows to determine internal magnetic fields at the position in the lattice where the muons stop. For a polycrystalline sample with a given static magnetic field B at the stopping site of the muon, the muon depolarization function[14] may be expressed as: $G_B(t) = \frac{1}{3} + \frac{2}{3}\cos(\gamma_\mu B t)$, where $\gamma_\mu = 2\pi \times 135.53$ MHz/T is the gyro-magnetic ratio of muon. $G_B(t)$ consists of two parts: a constant fraction of 1/3, and a fraction 2/3 oscillating with the frequency $\omega = \gamma_\mu B$. For a given magnetic field distribution $P(B)$, the muon depolarization function at the muon site is:[17]

$$G_P(t) = \frac{1}{3} + \frac{2}{3}\int_0^\infty P(B)\,\cos(\gamma_\mu B t)\,dB. \qquad (1)$$

The function $P(B)$ contains information on the magnetic structure and the spatial magnetic field distribution of the sample, but also the effect of a static electric field E on the local magnetic fields in the sample.

Due to an additional isotropic dynamic muon relaxation and the presence of a Cu background signal, the ZF depolarization function for Cu_2OSeO_3 is best described by the following equation:

$$A(t) = A_S \cdot \left(\frac{1}{3} + \frac{2}{3}\int_0^\infty P(B)\,\cos(\gamma_\mu B t + \phi)\,dB\right) e^{-\lambda t} + \\ + A_{Bg}\cdot G_{KT}(\sigma_{Bg} t)\cdot e^{-\lambda_{Bg} t}. \qquad (2)$$

Here A_S is proportional to the fraction of muons stopping in the sample, and A_{Bg} is proportional to the fraction of

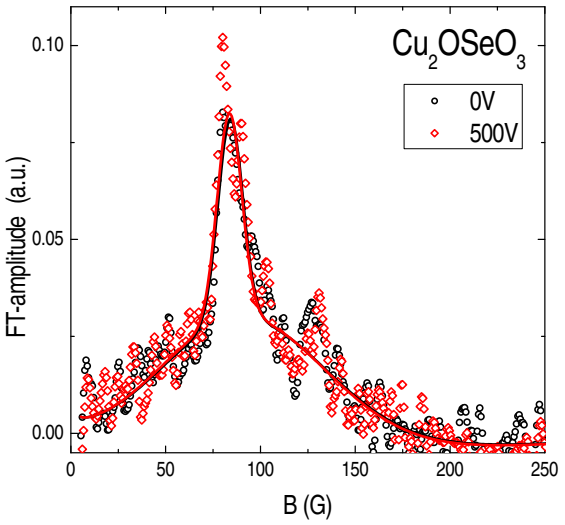

FIG. 2: (Color online) Fourier transform of the oscillating part of the asymmetry spectra shown in Fig. 1 (black circles: $E = 0$; red diamonds: $E = 500/3$ V/mm). The solid lines are the FT of the corresponding solid curves in Fig. 1

muons stopping in the Cu sample holder. The parameters λ_{Bg} and σ_{Bg} describe the temperature independent muon depolarization in Cu, while λ corresponds to the dynamic muon relaxation in the sample. $G_{KT}(\sigma_{Bg} t)$ denotes the Gaussian Kubo-Toyabe depolarization function.[18] Note that the phase $\phi = 0$ for zero field. As for a powder sample, we observe also for the present single crystal sample

a static fraction of 1/3 for the depolarization function and an oscillating fraction of 2/3.[14] In the case of a single crystal sample, though, these fractions are due to the formation of magnetic domains with a random spatial distribution which in fact corresponds to the situation for a polycrystalline sample. The best fit of $P(B)$ to the experimental data with a minimal set of parameters was obtained with a sum of two Gaussians:

$$P(B) = \sum_{i=1,2} \frac{F_S^i}{\sqrt{2\pi}\sigma_i/\gamma_\mu} \cdot \exp\left[-\frac{1}{2}\left(\frac{B-B_i}{\sigma_i/\gamma_\mu}\right)^2\right]. \quad (3)$$

Here F_S^1 and F_S^2 are the fractions of the two Gaussians with mean fields B_1 and B_2 and standard deviations σ_1/γ_μ and σ_2/γ_μ. Analysis of the data measured with highest statistics (100×10^6 positron events) at 10 K with Eqs. (2) and (3) [see Figs. (1) and (2)] yields in $F_S^1 = 0.18(2)$, $F_S^2 = 0.82(2)$, and $B_2/B_1 = 1.07(2)$ [note that $F_S^1 + F_S^2 = 1$]. The fit were performed by keeping all the sample parameters (A_S, σ_1, σ_2, λ, F_S^1, F_S^2, and B_2/B_1) and the background parameters (A_{Bg}, σ_{Bg}, and λ_{Bg}) the same, while $B_1(0\text{V})$ and $B_1(500\text{V})$ (data without and with the applied electric field) were free parameters. The temperature independent sample asymmetry $A_S = 0.144$ and the background parameters $A_{Bg} = 0.05$, $\sigma_{Bg} = 0.14(2)$ μs^{-1}, and $\lambda_{Bg} = 0.11(2)$ μs^{-1} were determined from the global fit of the whole temperature dependence, while the total initial asymmetry $A_S + A_{BG} = 0.194$ was determined above T_c. Further more, all the background parameters and the following sample parameters: F_S^1, F_S^2, B_2/B_1, were kept as temperature independent.

Figure 1 shows the asymmetry time spectra at 10 K and 58 K (below and above the magnetic transition) with and without electrostatic field E. The corresponding fits using Eqs. (2) and (3) are represented by the lines. Figure 2 shows the Fourier transform (FT) amplitudes of the oscillating part of the μSR spectra and the fitted curves shown in Fig. 1. For a small relaxation rate λ these FT amplitudes represent the magnetic field distribution $P(B)$ given by Eq. (3). Note that $P(B)$ consisting of two Gaussians [Eq. (3)] describes the basic features of the μSR spectrum quite well, and that the FT amplitudes for $E = 0$ and $E = 500/3$ V/mm are almost identical.

Before presenting the experimental results, we describe below the relation between the measured μSR spectra and the magnetic structure of Cu_2OSeO_3. The crystal symmetry of Cu_2OSeO_3 is cubic with a lattice constant $a = 8.9111$ Å and spatial group symmetry $P2_13$.[9] The lattice structure is thus quite complex with 32 oxygen ions in the unit cell, suggesting quite a large number of possible muon stopping sites. Generally, the positive muon stops at a high symmetry interstitial site of the lattice, close to negatively charged ions (in this case O^{2-}). In some cases the muon may form weak bonds with oxygen.[14] The function $P(B)$ describes the muon site-weighted distribution of internal fields in the sample.

In order to find the muon stopping sites, an analysis of the electrostatic potential was performed. The potential

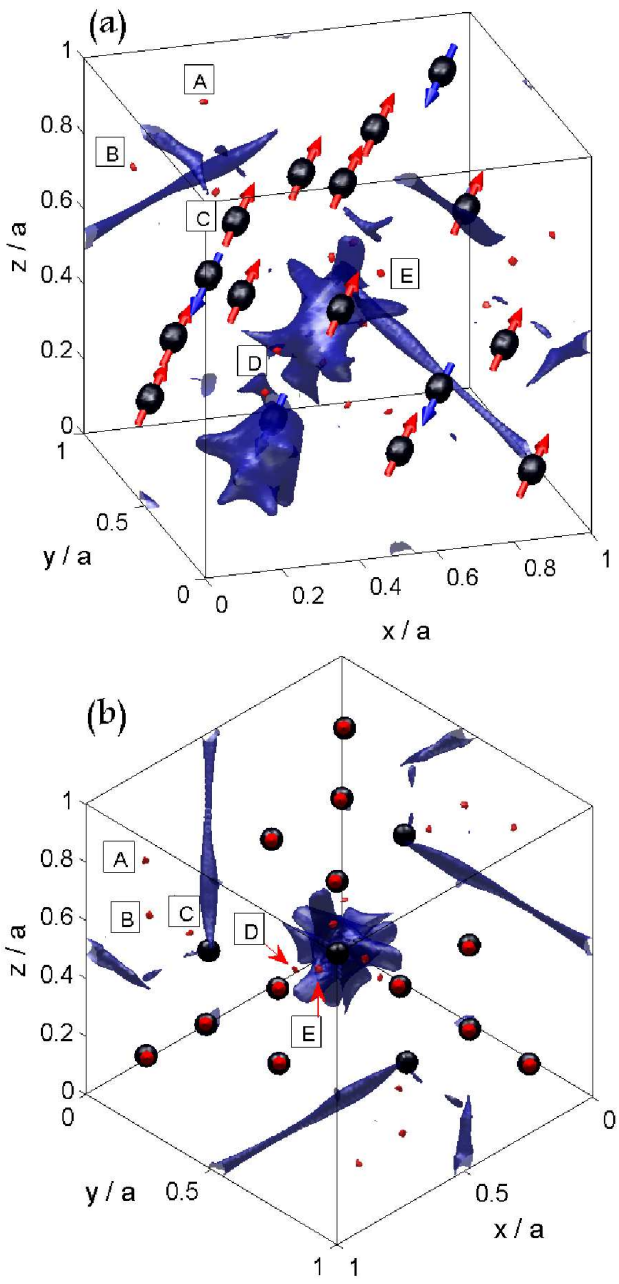

FIG. 3: (Color online) Magnetic structure and dipolar fields in Cu_2OSeO_3 (a). The black spherical surfaces represent a field strength of 20 T (i.e. Cu^{2+} ions). The arrows indicate the magnetic moments of Cu^{2+}. Blue surfaces represent internal fields of 10 mT (for $0.5\mu_B$ per Cu ion). The red spots A, B, C, D, and E are the muon stopping sites. Panel (b) shows the same as (a) but in the (111) direction.

at position $\mathbf{r}$ within the lattice unit cell was approximated using a spherical point charge-like model (in dimensionless units):

$$V(\mathbf{r}) = \sum_j \left(\frac{q_j}{R_j} + \frac{V_{xc}^0}{R_j} e^{-2R_j/R_j^I}\right). \quad (4)$$

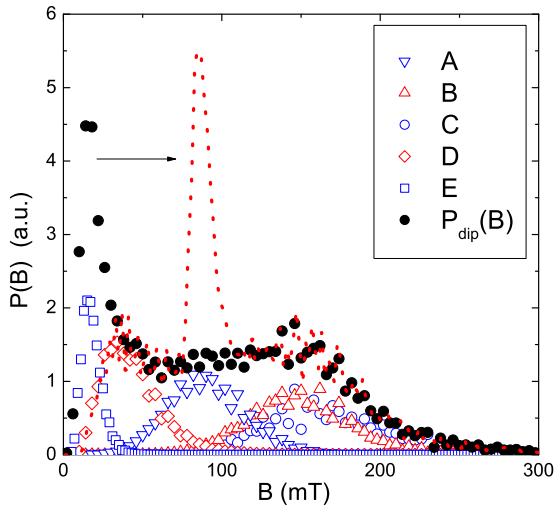

FIG. 4: (Color online) Probability distribution of dipolar fields $P_{\rm dip}(B)$ with equal weights for sites A, B, C, D, and E (•). The contributions of the individual sites A, B, C, D, and E to $P_{\rm dip}(B)$ are represented by the symbols, ▽, △, ○, ◇, and □, respectively. The width of each curve is proportional to the magnetic field gradient at the corresponding site. The dotted line shows the $P_{\rm dip}(B)$ with an additional contact field of 70 mT at site E.

The first term is the Coulomb potential, while the second term is the exchange correlation potential, which is usually assumed to be proportional to the local charge density (the expression $\exp(-R_j/R_j^I)$ represents an average radial wave function).[19,20] Here, $R_j = |\mathbf{r} - \mathbf{r}_j|$, and the sum is taken over ion coordinates $\mathbf{r}_j$ within a cluster of $4 \times 4 \times 4$ unit cells. The charges q_j and the ionic radii R_j^I are: +2 and 0.71 Å, +4 and 0.42 Å, −2 and 1.3 Å for Cu, Se, and O ions, respectively (here the elementary charge is unity). The adjustable parameter V_{xc}^0 was chosen as $\simeq +10$. We found that the coordinates of the potential minima do not appreciably depend on V_{xc}^0 over a broad range of values. The potential $V(\mathbf{r})$ has five magnetically non-equivalent minima with nearly equal depth at the following sites: A = (0.215,0.700,0.970), B = (0.035, 0.720, 0.805), C = (0.195, 0.555, 0.795), D = (0.275, 0.295, 0.460), and E = (0.635, 0.550, 0.525). The sites A, B, C, D, and E are indicated as red spots in Fig. 3. In addition, there are four local minima with higher energy and lower probability to be occupied.

The muon probes the vector sum of the internal (dipolar) magnetic field and the contact field at a particular lattice cite. The dipolar magnetic field $\mathbf{B}(\mathbf{r})$ at position $\mathbf{r}$ within the lattice unit cell is calculated as follows:[21]

$$B_{\rm dip}^{\alpha}(\mathbf{r}) = \frac{\mu_0}{4\pi} \sum_{i,\beta} \frac{m_i^{\beta}}{R_i^3} \left(\frac{3R_i^{\alpha} R_i^{\beta}}{R_i^2} - \delta^{\alpha\beta} \right). \qquad (5)$$

Here $\mathbf{R}_i = \mathbf{r} - \mathbf{r}_i$, α and β denote the vector components x, y, and z, $\mathbf{r}_i$ is the position of i-th magnetic ion in the unit cell, and m_i^{β} is the corresponding dipolar moment. The summation is taken over a sufficiently large Lorentz sphere of radius R_L. Beyond the Lorentz sphere, the integration is carried out over the domain volume. The contribution to the internal magnetic field from this integral is $\mathbf{B}' = 4\pi\mu_0(\frac{1}{3} - \hat{\mathbf{N}}_{\mathbf{d}})\mathbf{M}$,[22] where $\mu_0\mathbf{M} \simeq 66$ mT is the domain magnetization, and $\hat{\mathbf{N}}_{\mathbf{d}}$ the demagnetization tensor determined by the geometry of the domain and the magnetic anisotropy. For the calculation of the magnetization the lattice constant $a = 8.91113$ Å and the magnetic moment of $0.5\mu_B$ per Cu^{2+} ion were taken from Ref. 9. For a magnetically isotropic spherical domain $\hat{\mathbf{N}}_{\mathbf{d}} = \frac{1}{3}$.[21,22] The field $\mathbf{B}'$ and the stray fields due to the neighboring domains average statistically to zero. They only give rise to an additional broadening of $P(B)$, which is smaller than the width of the narrow component of $P(B)$ (see Fig. 2). The magnetic structure of Cu_2OSeO_3 and the spatial magnetic field distribution calculated with Eq. (5) is shown in Fig. 3. The probability field distributions for the magnetic structure with equal weights for the muon sites A, B, C, D, and E are shown in Fig. 4. The calculations were performed with Gaussian sampling around the points A, B, C, D, and E, with a standard deviation $\sigma_L = 0.23$ Å. Thus, the widths of the curves in Fig. 4 are proportional to the magnetic field gradients at the corresponding sites. The total field distribution from all sites A, B, C, and D has a broad Gaussian-like shape centered at approximately 100 mT. This broad distribution agrees quite well with the experimental distribution (see Fig. 2). The narrow peak calculated for site E is located at about 15 mT, in contrast to the experimentally observed peak at around 85 mT. This discrepancy may be explained by assuming an additional contact field of approximately 70 mT at the muon site E, resulting in a peak position of 85 mT (the total field is the vector sum of the dipolar field $\mathbf{B}_{\rm dip}$ and the contact field $\mathbf{B}_c$). Note that the ratio of the broad and the narrow signal intensities is about 4, in good agreement with the ratio $F_S^2/F_S^1 = 4.5(5)$ obtained from Eq. (3) above.

IV. RESULTS AND DISCUSSION

The temperature dependence of the parameters σ_1, σ_2, and λ as obtained from the data analysis by means of Eqs. (2) and (3) are displayed in Fig. 5. The parameters σ_1 and σ_2 decrease with increasing temperature and drop to zero at the Curie temperature $T_c = 57.0(1)$ K of the ferrimagnetic transition of Cu_2OSeO_3. The longitudinal relaxation rate λ is a measure of the internal magnetic field dynamics and can be expressed by the field-field correlation function $\lambda = \gamma_\mu^2 \int_0^\infty < B_\perp(t)B_\perp(0) > dt$.[23] Here $B_\perp$ is the field component perpendicular to the muon-spin direction at the muon site. Brackets denote statistical averages. In the paramagnetic state close to T_c the relaxation rate λ is a measure of the spatial correlation length ξ of the magnetic order. In the critical state the

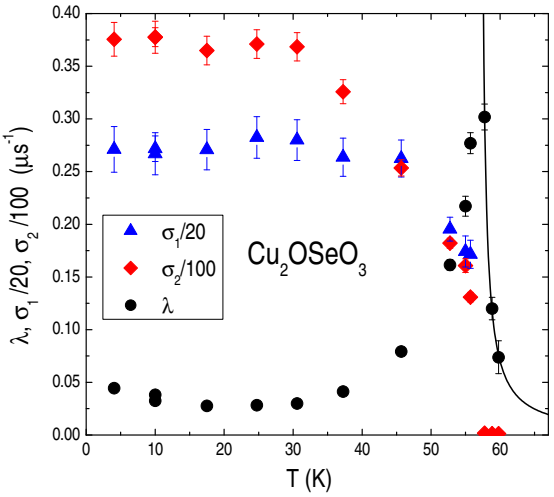

FIG. 5: (Color online) Transverse relaxation rates σ_1 and σ_2 as well as longitudinal relaxation rate λ of single-crystal Cu_2OSeO_3 as a function of temperature. The black solid line represents a fit of the data to the power law $\lambda(T) = A(T/T_c - 1)^{-\tilde{\omega}}$ (see text).

following relations hold: $\lambda \propto \xi^{3/2}$ for ferromagnets and $\lambda \propto \xi^{1/2}$ for antiferromagnets.[24–26] Note that these relations are only strictly valid in the critical regime very close to T_c. However, it was found empirically, that these relations describe experimental data rather well for EuO, EuS, $RbMnF_3$ up to $\sim 1.3T_c$.[25,26] Above T_c the correlation length ξ follows the power low $\xi \propto (T/T_c - 1)^{-\tilde{\nu}}$, where the effective critical exponent $\tilde{\nu} \simeq 0.70$ for a 3D Heisenberg magnet.[24–26] A fit of λ above T_c to the equation $\lambda(T) = A(T/T_c - 1)^{-\tilde{\omega}}$ results in $A = 0.0030(5)$ μs^{-1} and the effective dynamic exponent[29] $\tilde{\omega} = 1.06(9)$ (see the black line in Fig. 5). Thus, for $\tilde{\nu} \simeq 0.70$, we find with $\tilde{\omega}/\tilde{\nu} = 1.5$ that $\lambda \propto \xi^{1.5}$, in fair agreement with the critical behaviour of a 3D ferromagnet ($\lambda \propto \xi^{3/2}$).

Next we discuss the μSR experiments with an electric field applied. The temperature dependence of the mean internal magnetic field B_1 with or without applied electric field E is shown in Fig. 6(a). The temperature dependence of the internal magnetic field (i.e. the magnetic order parameter) decreases with increasing temperature and vanishes at T_c. Analyzing the data with the power law:[23]

$$B_1 = B_1(0) \cdot (1 - (T/T_c)^{\tilde{\alpha}})^{\tilde{\beta}} \qquad (6)$$

yields $T_c = 57.0(1)$ K, $\tilde{\alpha} = 2.00(9)$, $\tilde{\beta} = 0.39(1)$, and $B_1(0) = 85.37(25)$ and $85.57(25)$ mT for $E = 0$ and $500/3$ V/mm, respectively. The value of the effective critical expoment[29] $\tilde{\beta}$ lies quite close to the critical exponent $\beta \simeq 1/3$ expected for a 3D magnetic system.[27] For $T \to 0$ the temperature dependence of the internal field $B_1(0) - B_1(T) \propto T^{\tilde{\alpha}}$ is determined by the excitation of the ground state magnetic order.[27,28] Figure 6(b) shows

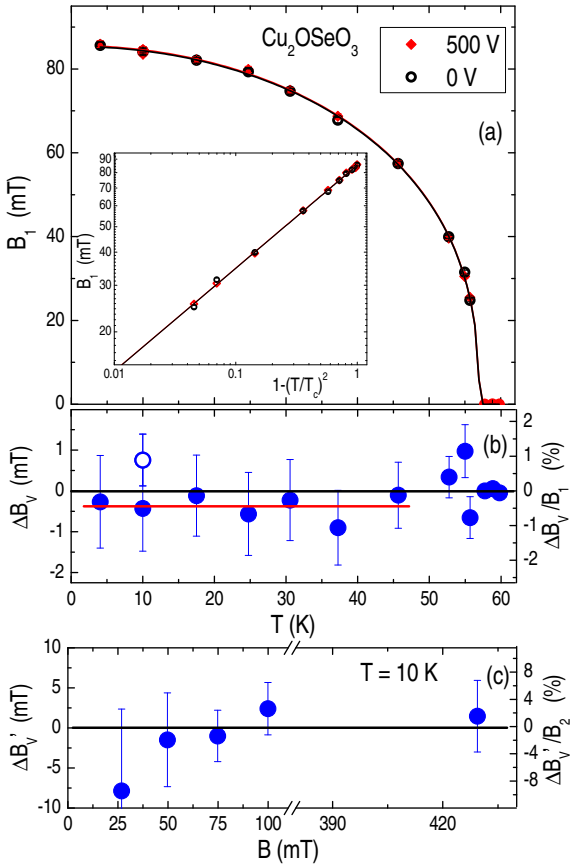

FIG. 6: (Color online) (a) Temperature dependence of the mean internal B_1 field in single crystal Cu_2OSeO_3 for zero and applied electrostatic field E. The solid lines are power law fits to the data with Eq. (6). The insert shows B_1 vs $(1-(T/T_c)^2)$ on a log-log scale.(b) Electric field shift $\Delta B_V = B_1(0V) - B_1(500V)$ as a function of temperature. The solid red line corresponds to the mean value of $\overline{\Delta B_V} \simeq -0.4(4)$ mT below 50 K. (c) Electric field shift $\Delta B'_V = \hat{B}_2(0V) - \hat{B}_2(800V)$ as a function of magnetic field measured in the TF μSR experiment at 10K.

the difference $\Delta B_V = B_1(0V) - B_1(500V)$ as a function of temperature. Obviously, the data points scatter substantially. However, a close examination shows that the data points below 50 K are systematically shifted to negative values, except of a point at 10 K [the blue open circle in Fig. 6(b)] which is the first measured point and it was recorded in the test phase of the experiment. Thus, we cannot exclude additional systematic errors related to instrument set up for the first point. The statistical average of all values of ΔB_V is zero within error. By excluding the data point at 10 K the average value $\overline{\Delta B_V}$ below 50 K was found to be $\simeq -0.4(4)$ mT. These experiments suggest the presence of a small electric field effect on the magnetic state of Cu_2OSeO_3.

Additional μSR experiments were performed with an

applied transverse magnetic field (TF). The μSR spectra were found to be well described by the asymmetry function:

$$A_{TF}(t) = \hat{A}_S \exp\left(-\frac{1}{2}\hat{\sigma}_2^2 t^2\right)\cos(\gamma_\mu \hat{B}_2 t + \phi) + \\ + \hat{A}_{Bg} \exp\left(-\frac{1}{2}\hat{\sigma}_{Bg}^2 t^2\right)\cos(\gamma_\mu \hat{B}_{Bg} t + \phi). \quad (7)$$

The parameter $\hat{A}_S(\hat{A}_{Bg})$ corresponds to $A_S(A_{Bg})$ in Eq. (2), while $\hat{\sigma}_2(\hat{\sigma}_{Bg})$ and $\hat{B}_2(\hat{B}_{Bg})$ are the relaxation rate and the mean field of the sample (Cu background), respectively. The values of $\hat{\sigma}_2$ and σ_2 were found to be approximately the same, and the Cu relaxation rate $\hat{\sigma}_{Bg} \simeq 0.25\ \mu\mathrm{s}^{-1}$ is small. $\hat{B}_2$ is slightly larger than the applied field, while $\hat{B}_{Bg}$ is close to the applied field. In the TF μSR experiments the electric field amplitude was increased to 800/3 V/mm. Note that the signal from the sample is well described by a single Gaussian, and that the narrow signal in Eq. (3) broadens. The field dependence of $\Delta B'_V = \hat{B}_2(0\mathrm{V}) - \hat{B}_2(800\mathrm{V})$ at $T = 10$ K is shown in Fig. 6(c). No effect of the electric field E on the internal magnetic field was found within the precision of the experiment, although a strong field dependence of the magneto-capacitance was reported.[9] The TF μSR experiment is less precise than the ZF experiment, since the narrow signal that mainly determines the errors becomes broader by applying a magnetic field.

V. CONCLUSION

In conclusion, we performed a detailed investigation of magnetism and the magneto-electric effect in Cu_2OSeO_3 by ZF and TF μSR. An internal magnetic field $B_{\mathrm{int}}(T = 0) = 85.37(25)$ mT was detected below $T_c = 57.0(1)$ K, consistent with a ferrimagnetic state.[9] The effective critical exponent for the temperature dependence of B_{int} was found to be $\tilde{\beta} \simeq 0.39(1)$, in fair agreement with the critical exponent $\beta \simeq 1/3$ expected for 3D magnetic systems. The magnetic order parameter $B(0) - B(T) \propto T^2$ was found to exhibit a quadratic temperature dependence for $T \to 0$. The temperature dependence of the muon relaxation rate above T_c is well described by the relation $\lambda \propto (T/T_c - 1)^{-\tilde{\omega}}$ with $\tilde{\omega} = 1.06(9)$, suggesting $\lambda \propto \xi^{3/2}$ (ξ is the magnetic correlation length) which is characteristic for 3D ferromagnets.[24,25] The ZF μSR measurements of the microscopic internal field distribution with and without applied electric field $E = 500/3$ V/mm indicate a small electric field effect on the internal magnetic field: $\Delta B_V = B_1(0\mathrm{V}) - B_1(500\mathrm{V}) = -0.4(4)$ mT. The strong muon relaxation sets a limit on the precision of detecting a magneto-electric effect. To improve the precision of the μSR experiment substantially higher statistics would be needed.

VI. ACKNOWLEDGEMENTS

We are grateful to A. Amato and A. Raselli for their technical support during the μSR experiments. Discussions with P.F. Meier on possible muon sites are acknowledged. This work was performed at the Swiss Muon Source (SμS), Paul Scherrer Institut (PSI, Switzerland). We acknowledge support by the Swiss National Science Foundation and the NCCR *Materials with Novel Electronic Properties* (MaNEP).

* Electronic address: alexander.m@physik.uzh.ch

[1] M. Fiebig, J. Phys. D: Appl. Phys. **38** R123 (2005).
[2] N. A. Spaldin and M. Fiebig, Science **309**, 391 (2005).
[3] W. Eerenstein, N.D. Mathur, and J.F. Scott, Nature **442**, 759 (2006).
[4] S.-W. Cheong and M. Mostovoy, Nature Materials **6**, 13 (2007).
[5] N. A. Hill, J. Phys. Chem. B **104**, 6694 (2000).
[6] G. A. Gehring, Ferroelectrics **161**, 275 (1994).
[7] I. A. Sergienko and E. Dagotto, Phys. Rev. B **73**, 094434 (2006).
[8] H. Katsura, N. Nagaosa, and A. V. Balatsky, Phys. Rev. Lett. **95**, 057205 (2005).
[9] J.-W. G. Bos, C. V. Colin, and T. T. M. Palstra, Phys. Rev. B **78**, 094416 (2008).
[10] H. Effenberger and F. Pertlik, Monatsch. Chem. **117**, 887 (1986).
[11] M. Belesi, I. Rousochatzakis, H. C. Wu, H. Berger, I. V. Shvets, F. Mila, and J. P. Ansermet, Phys. Rev. B **82**, 094422 (2010).
[12] K. H. Miller, X. S. Xu, H. Berger, E. S. Knowles, D. J. Arenas, M. W. Meisel, and D. B. Tanner, Phys. Rev. B **82**, 144107 (2010).
[13] V. Gnezdilov, K. Lamonova, Y. Pashkevich, P. Lemmens, H. Berger, F. Bussy, and S. Gnatchenko, Fiz. Nizk. Temp. **36**, 688 (2010).
[14] S. J. Blundell, Contemporary Physics **40**, 175 (1999).
[15] D. G. Eshchenko, V. G. Storchak, and G. D. Morris, Phys. Lett. A **264**, 226 (1999).
[16] H. J. Lewtas, T. Lancaster, P. J. Baker, S. J. Blundell, D. Prabhakaran, and F. L. Pratt, Phys. Rev. B **81**, 014402 (2010).
[17] P. Carretta and A. Keren, arXiv:0905.4414v1 (2009).
[18] R. Kubo, Hyperfine Int. **104**, 3 (1997).
[19] S. Estreicher and P. F. Meier, Phys. Rev. B **27**, 642 (1983).
[20] G. J. M. Velders and D. Feil, Acta Cryst. **B45**, 359 (1989).
[21] S. J. Blundell, Physica B **404**, 581 (2009).
[22] R. M. White, *Quantum Theory of Magnetism* (McGraw-Hill, New York, 1970).
[23] F. L. Pratt, P. M. Zieliński, M. Balanda, R. Podgajny, T. Wasiutyński, and B. Sieklucka, J. Phys. Condens. Matter, **19**, 456208 (2007).

[24] A. Yaouanc, P. Dalmas de Réotier, and E. Frey, Phys. Rev. B **47**, 796 (1993).
[25] S. W. Lovesay and E. Engdahl, J. Phys.: Condens. Malter **7**, 769 (1995).
[26] S.W. Lovesay, B. Balcar, and A. Cuccoli, J. Phys.: Condens. Malter **7**, 2615 (1995).
[27] L. J. De Jongh and A. R. Miedema, Advan. Phys. **23**, 1 (1974).
[28] L. P. Le, A. Keren, G. M. Luke, W. D. Wu, Y. J. Uemura, M. Tamura, M. Ishikawa and M. Kinoshita, Chem. Phys. Lett. **206**, 405 (1993).
[29] H. Keller and I. M. Savić, Phys. Rev. B **28**, 2638 (1983).